Electrical properties of Er-doped $In_{0.53}Ga_{0.47}As$

Peter G. Burke,[a] Hong Lu, Nicholas G. Rudawski, and Arthur C. Gossard
Materials Department, University of California, Santa Barbara, California 93106

Je-Hyeong Bahk and John E. Bowers
Electrical and Computer Engineering Department, University of California, Santa Barbara, California 93106

(Received 28 October 2010; accepted 3 February 2011; published 3 March 2011)

The electrical properties of $In_{0.53}Ga_{0.47}As$ thin films Er-doped to concentrations of 1.5×10^{17}–7.2×10^{20} cm^{-3} grown by molecular beam epitaxy at 490 °C on (001) InP substrates were studied. Electrical conductivity, carrier density, and carrier mobility as a function of Er doping were measured by Hall effect at temperatures of 20–750 K. Additionally, high-angle annular dark-field scanning transmission electron microscopy and infrared absorption spectroscopy confirmed the presence of epitaxially embedded ErAs nanoparticles at Er concentrations $\geq 8\times10^{19}$ cm^{-3}. The observed electrical properties are discussed in terms of the dependence of ErAs nanoparticle formation with Er doping. © *2011 American Vacuum Society.* [DOI: 10.1116/1.3559480]

I. INTRODUCTION

The luminescence of semiconductors doped with rare-earth elements is of significant technological interest[1] because it provides spectra with sharp, narrow emission lines whose positions are largely insensitive to temperature. This emission comes from internal *f* shell transitions in the rare-earth atom, which are close to the atom core and almost independent of the surrounding matrix.[2] Er is particularly interesting because its characteristic emission[3] occurs at a wavelength of 1.54 μm, which is useful for Si-based optical communication applications.[4] However, rare-earth elements, such as Er, have not been extensively studied for their properties as electrically active dopants in narrow band gap III-V semiconductors.

The electronic properties of Er-doped III-V semiconductors, such as $In_{0.53}Ga_{0.47}As$, are of great interest for applications such as thermoelectric power generation.[5] Materials used for thermoelectric applications are evaluated by the unitless figure of merit,[6]

$$ZT = \frac{S^2\sigma}{\kappa}, \tag{1}$$

where S is the Seebeck coefficient, σ is the electrical conductivity, and κ is the total thermal conductivity comprised of contributions from both lattice phonons and the movement of charge carriers. Therefore, it is important to understand how doping a III-V semiconductor with Er can potentially change the electronic and thermal properties of the material.

It is known that incorporating Er into III-As based semiconductors during growth by molecular beam epitaxy (MBE) causes embedded, coherent, rocksalt ErAs clusters to form in the shape of particles,[7] rods,[8] and even "trees."[9] These embedded nanoparticles can decrease the thermal conductivity compared to semiconductors of similar doping without nanoparticles[10,11] and potentially increase the Seebeck coefficient through electron filtering.[12] It was also shown that these nanoparticles can donate electrically active carriers and that the Fermi level shifts with respect to the undoped $In_{0.53}Ga_{0.47}As$ conduction band edge, depending on the size of the nanoparticle.[13] However, the dopant behavior of dilute Er atoms in MBE-grown $In_{0.53}Ga_{0.47}As$ has never been examined. The doping of Er and Yb in InP was studied by Lambert *et al.*[14] but their explanation of carrier donation never considered ErP nanoparticles. Also, the fact that InP has nearly twice the band gap of $In_{0.53}Ga_{0.47}As$ makes the situation very different. The nanoparticle formation composition limit was identified as 7×10^{17} cm^{-3} for MBE-grown GaAs,[7] but the limit in $In_{0.53}Ga_{0.47}As$ could be different due to the different host lattices and the different growth conditions. Specifically, $In_{0.53}Ga_{0.47}As$ has a larger lattice constant (a=5.87 Å) compared to GaAs (a=5.65 Å), which would imply a lower energy for substitutional defects.[15] Also, $In_{0.53}Ga_{0.47}As$ is grown at a lower growth temperature of ~490 °C as compared to GaAs, which was grown at 580 °C in the prior study.[7]

At higher Er concentrations where semimetallic nanoparticles form, the nanoparticles can donate electrons to the matrix if the Fermi level of the ErAs particle is near or above the conduction band edge of the bulk $In_{0.53}Ga_{0.47}As$. Furthermore, Zimmerman *et al.*[16] demonstrated that the barrier height of ErAs on $In_xGa_yAl_{1-x-y}As$ films could be tuned with the composition of the matrix. By assuming that these barriers are inherently the same for ErAs nanoparticles epitaxially embedded in bulk $In_xGa_yAl_{1-x-y}As$, the nanoparticles can contribute electrons to the host matrix. In this work, the structural and electrical properties of Er-doped $In_{0.53}Ga_{0.47}As$ were studied for a wide range of Er concentrations to investigate the possibility of using Er as a dopant in narrow band gap III-V semiconductors.

[a]Electronic mail: peterburke@umail.ucsb.edu; American Vacuum Society member.

II. EXPERIMENTAL PROCEDURES

$In_{0.53}Ga_{0.47}As$ films were grown on 600-μm-thick semi-insulating (001) InP substrates by MBE at 490 °C on a solid-source system with an As_2:III flux ratio of ~20:1 and a growth rate of ~2 μm/h. For each sample, the substrate native oxide was desorbed under As_2 flux at 550 °C and a 100-nm-thick $In_{0.52}Al_{0.48}As$ buffer layer was grown to smoothen the growth surface. Also, $In_{0.52}Ga_{0.48}As$ has a larger band gap than $In_{0.53}Ga_{0.57}As$, which provides an electronic barrier to isolate the epilayer from the substrate during Hall effect measurements. Subsequently, the Er-doped $In_{0.53}Ga_{0.47}As$ layer (active layer) was grown to a thickness of ~2 μm and left uncapped. Both the buffer and the active layer were grown under InP lattice matching conditions, which was confirmed with high resolution x-ray diffraction. The Er concentration was calculated by measuring the growth rate of ErSb thin films on GaSb and by measuring the Er signal in Rutherford backscattering spectrometry.[17,18]

High-angle annular dark-field scanning transmission electron microscopy (HAADF-STEM) using an FEI Titan microscope operated with an accelerating voltage of 300 kV and a convergence semiangle of 9.6 mrad was used to directly image the atomic-level structure of the films. The method of sample preparation is provided elsewhere.[19] The sample thickness of the imaged areas was estimated at 15 ± 3 nm, as determined by position-averaged convergent beam electron diffraction[20] with a total search area of ~4 μm^2 for each sample.

Additionally, infrared absorption spectroscopy was used to study the structure of the samples since it is known that the ErAs nanoparticles exhibit strong plasmon resonance.[21] Infrared absorption spectra were obtained using a Cary 500 spectrophotometer, scanning from 3000 to 800 nm. The parameters used were an averaging time of 0.1 s, a data interval of 1nm, a scan rate of 600 nm/min, and a slit bandwidth of 2 nm. The setup geometry was such that the generated beam was transmitted through the sample, perpendicular to the epilayer.

Finally, the electrical properties of the films were studied using Hall effect measurements with samples prepared by standard lithography techniques. Mesas were wet-etched using a 15:5:1 volume ratio of ($DI:H_2O_2:H_3PO_4$) and then capped with passivation layers (200 nm SiN_x/100 nm SiO_2) deposited by plasma enhanced chemical vapor deposition. Sputtered metallization layers of 50 nm $TiWN_x$ and 500 nm Au were used due to provided stability[22] at temperatures up to 750 K introduced during electrical measurements.

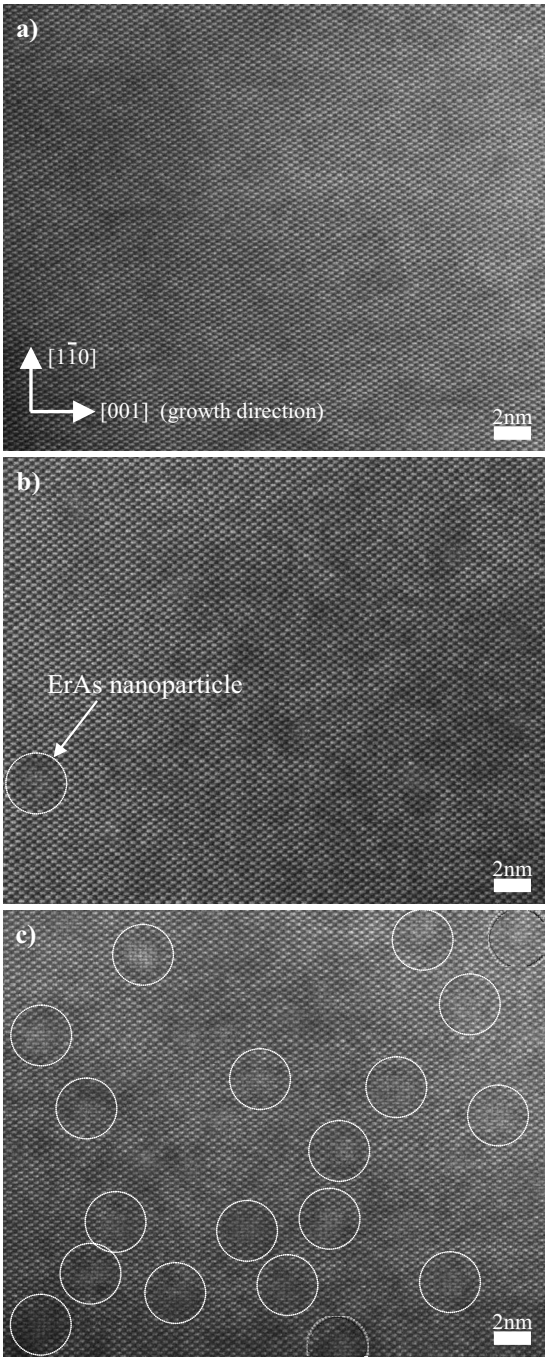

FIG. 1. HAADF-STEM images of (a) 2×10^{19} cm^{-3}, (b) 8×10^{19} cm^{-3}, and (c) 7.2×10^{20} cm^{-3} Er-doped $In_{0.53}Ga_{0.47}As$ samples taken along the [110] zone axis. The nanoparticles are loosely circled for easy identification. The lowest concentration at which nanoparticles could be identified was 2×10^{19} cm^{-3}.

III. RESULTS

A. High-angle annular dark-field scanning transmission electron microscopy results

HAADF-STEM was used to study the effect of Er doping on the atomic-level structure of $In_{0.53}Ga_{0.47}As$, as shown in Fig. 1. In the case of Er doping of 2×10^{19} cm^{-3}, shown in Fig. 1(a), ErAs nanoparticles were not observed. With increased Er doping of 8×10^{19} cm^{-3}, shown in Fig. 1(b), occasional isolated nanoparticles were observed. However, at an Er concentration of 7×10^{20} cm^{-3}, nanoparticles were observed very frequently. Considering the approximate sample thickness of 15 ± 3 nm and the 4 μm^2 search area, the densities of nanoparticles were estimated to be $\leq 2 \times 10^{17}$, ~2×10^{17}, and ~2×10^{18} cm^{-3} for Er concentrations of 2×10^{19}, 8×10^{19}, and 7.2×10^{20} cm^{-3}, respectively. Thus, it

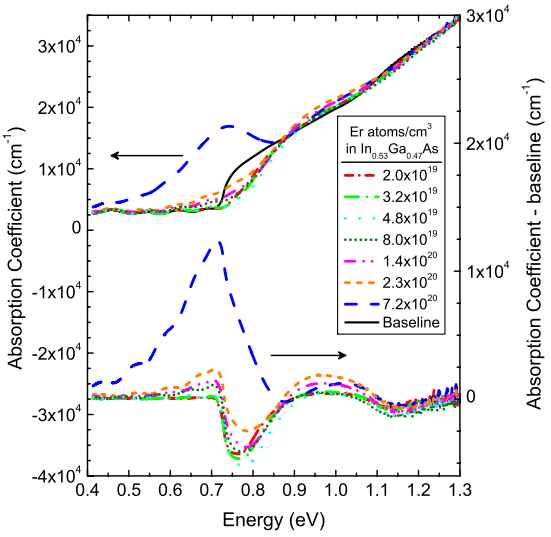

FIG. 2. (Color online) Infrared absorption coefficient measured at room temperature. The intensity of the plasmon absorption peak at ~0.72 eV increases with increasing Er concentration. A scan from undoped $In_{0.53}Ga_{0.47}As$ on InP is subtracted as a baseline.

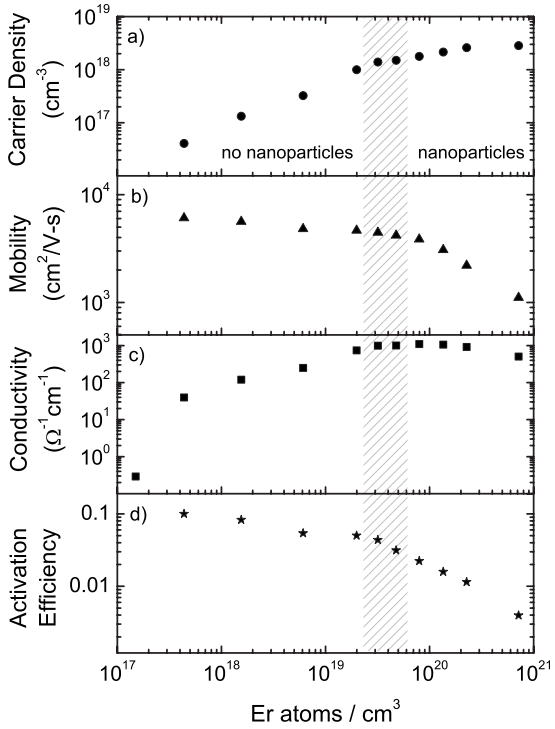

FIG. 3. Room temperature Hall effect measurements on Er-doped $In_{0.53}Ga_{0.47}As$. The shaded area indicates the concentration limit at which nanoparticles form for the given MBE growth conditions.

is advanced that ErAs nanoparticle formation does not occur below Er concentrations of 2×10^{19} cm^{-3}. These findings are consistent with a previous conclusion by Sethi and Bhattacharya[23] that nanoparticles do not form below a similar concentration in MBE-grown Er-doped $In_{0.53}Ga_{0.47}As$.

B. Infrared absorption measurement results

Infrared absorption spectroscopy was also used to study the structure of the films as a function of Er concentration and detect the presence of ErAs nanoparticles, as shown in Fig. 2. The absorption coefficient, α, was calculated as

$$\alpha = -\frac{1}{t}\ln\left(\frac{T}{T_0}\right), \tag{2}$$

where t is the thickness of the active $In_{0.53}Ga_{0.47}As$ layer, T is the transmitted intensity through the measured sample, and T_0 is the chosen transmitted intensity baseline.[24] Since the active layer in this case is potentially composed of semimetallic nanoparticles coherently embedded in a semiconductor matrix,[25,26] the transmitted intensity from the epilayer is a combination of contributions from the nanoparticles and the semiconductor matrix. To isolate the contribution from ErAs nanoparticles, a baseline of undoped $In_{0.53}Ga_{0.47}As$ on InP was subtracted from the as-measured Er-doped $In_{0.53}Ga_{0.47}As$ spectra. As shown in Fig. 2, a clear peak at 0.72 eV is evident for samples with Er concentrations $\geq 8\times10^{19}$ cm^{-3} and not evident for the samples with an Er concentration of $\leq 4.8\times10^{19}$ cm^{-3}.

Absorption peaks attributed to surface plasmon resonances have been seen before for metallic particles in different media[27] as well as for ErAs nanoparticles embedded in GaAs.[21,24,28] In the present case, the peaks shown in Fig. 2 are likely due to the presence of semimetallic nanoparticles in the semiconductor film. While metallic nanoparticles show plasmon peaks in the visible or ultraviolet range, semimetallic nanoparticles have lower carrier densities and thus have plasmon peaks in the infrared regime.[29–33]

C. Hall effect measurement results

The influence of Er doping on carrier density, carrier mobility, and conductivity of $In_{0.53}Ga_{0.47}As$ films was determined using room temperature Hall effect measurements, as shown in Fig. 3. As expected, the carrier density increases with Er doping, as shown in Fig. 3(a), while the carrier mobility decreased with Er doping, as shown in Fig. 3(b). The conductivity reaches a maximum at an Er concentration of $\sim 8\times10^{19}$ cm^{-3}, as shown in Fig. 3(c). The activation efficiency (ratio of active carriers to dopant atoms) of Er in $In_{0.53}Ga_{0.47}As$, indicated in Fig. 3(d), is highest, ~10%, for the lowest dopant levels and decreases with Er doping. It should be noted that the trend lines presented in Fig. 3 exhibit a significant change in slope at $\sim 6\times10^{19}$ cm^{-3}, which is within the range of concentrations for which nanoparticles are expected to form for the given growth conditions.

Figure 4 presents the temperature dependence of the electrical properties of $In_{0.53}Ga_{0.47}As$ with different levels of Er doping as determined using Hall effect measurements. While the conductivity, shown in Fig. 4(c), does flatten out unexpectedly from ~250 to 300 K, the carrier density, shown in Fig. 4(b), and carrier mobility, shown in Fig. 4(a), which are calculated from the Hall coefficients, exhibit stronger anomalies. Since the Hall analysis assumes only one type of carrier and a homogeneous material, it is very possible that

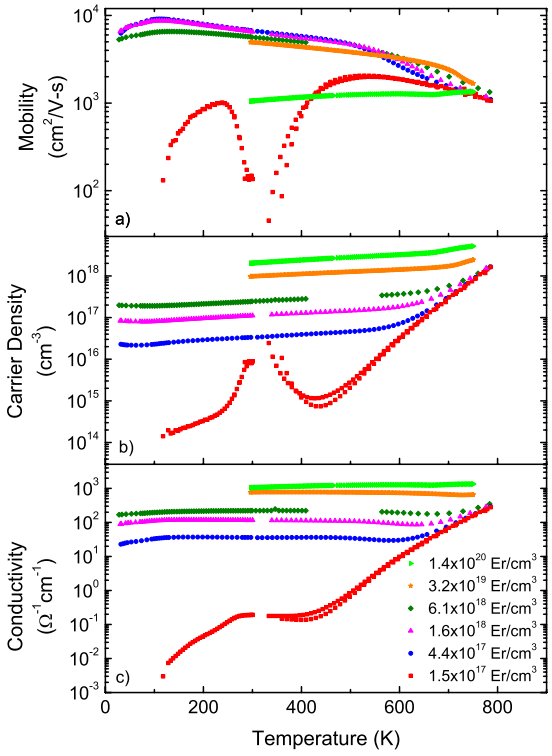

FIG. 4. (Color online) Temperature dependent (a) carrier mobility, (b) carrier density, and (c) conductivity, as measured by the Hall effect.

the calculated carrier density and mobility are incorrect for the most resistive sample. It should be noted that the most conductive sample in Fig. 4, Er doping of 1.4×10^{20} cm^{-3}, was the only sample known to have ErAs nanoparticles, and it exhibited decreasing carrier mobility with decreasing temperature. All of the other samples, with the exception of the lowest doped sample, show an increase in mobility with temperature to a maximum observed near ~100 K. The carrier density for each sample drops slowly with decreasing temperature, and the conductivity stays relatively constant from ~100 to 550 K. Above ~550 K, the carrier density and conductivity suddenly change behavior and start rapidly increasing. This increase in conductivity likely occurs because the semi-insulating InP substrate gains thermally excited intrinsic carriers and is nearly 300 times thicker than the epilayer. Therefore, the conductivity through the substrate dominates the measurement. This effect becomes dominant at higher temperatures for highly doped samples, ~650 K, but relatively low for the most dilute sample, ~550 K.

The natural log of the carrier density versus reciprocal temperature is plotted in Fig. 5 in order to estimate the activation energy of the donor dopant acting in this system. For the samples with Er doping $\geq4.4\times10^{17}$ cm^{-3}, carrier freeze out was not observed down to a temperature of 25 K. Carrier freeze out behavior, along with an unexplained peak in carrier density near room temperature, was observed in the most dilute sample with an Er concentration of 1.5×10^{17} cm^{-3}. The activation energy for Er in $In_{0.53}Ga_{0.47}As$ can be estimated given the Arrhenius temperature dependence of excited carriers across an energy gap. The slope of the curve

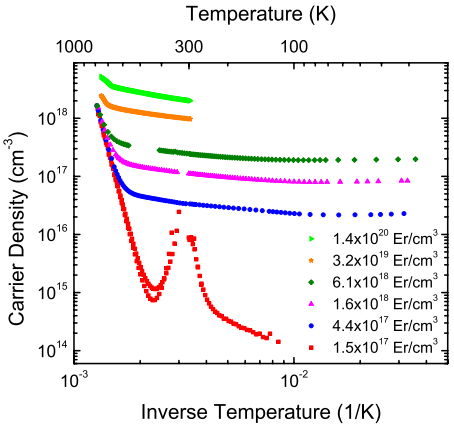

FIG. 5. (Color online) Natural log of the carrier density vs reciprocal temperature for Er-doped $In_{0.53}Ga_{0.47}As$ MBE-grown thin films with and without ErAs nanoparticles. The activation energy is calculated using the linear slope of the curves below 200 K.

representing the lowest doped sample below 200 K gives an activation energy of $E_d\sim25$ meV below the conduction band edge, making Er a shallow-type donor in $In_{0.53}Ga_{0.47}As$. The slopes of the curves representing the higher doped samples are nearly horizontal and yield an activation energy of $E_d\sim4$ meV. This implies that $In_{0.53}Ga_{0.47}As$ with Er doping higher than 4.4×10^{17} cm^{-3} becomes degenerately doped possibly due to Er atoms forming an impurity band[34] or shifting the conduction band edge.[35] At high temperatures, the slopes of the samples approaches ~1.5 eV, which is consistent with the hypothesis that the InP substrate dominates the measurement at higher temperatures.

IV. DISCUSSION OF ERBIUM AS A DONOR

Er and group III elements, such as Ga and In, most commonly exist in the 3^+ oxidation state in stable compounds, such as ErF_3, GaF_3, GaAs, InAs, and others. Therefore, Er can be considered to be isovalent with Ga and In.[36] If Er codeposited in $In_{0.53}Ga_{0.47}As$ by MBE is a substitutional defect on a cation site, it should not add an electrically active carrier to the semiconductor matrix. However, MBE-grown Er-doped $In_{0.53}Ga_{0.47}As$ samples have more conductivity than undoped $In_{0.53}Ga_{0.47}As$. One explanation for this observation is that Er exists as Er^{4+} ($4f^{10}$ configuration) instead of Er^{3+} ($4f^{11}$ configuration) in $In_{0.53}Ga_{0.47}As$. This might be the case if Er^{4+} is more energetically favorable than Er^{3+} at high temperatures. Also, Er may occupy an interstitial site and act as a donor in $In_{0.53}Ga_{0.47}As$.

In order to refute that impurities may be the source of doping, secondary ion mass spectrometry was conducted on each as-grown sample and impurities were not detected above the detection limit of the measurement, which is $\sim10^{15}$ cm^{-3}, depending on the ionizability of the element in question. Also, the Er source material provided by Ames Laboratory was analyzed by SHIVA Technologies using glow-discharge mass spectrometry (GDMS) to determine the concentration of impurity elements. The elements present in the highest concentrations included Pb (5.6 ppm wt or 5

$\times 10^{-4}$ at. %), Fe (2ppm wt), W (2 ppm wt), Nd (0.93 ppm wt), and Ho, Tm Cu, Cr, Al (all ~0.62 ppm wt).[37] These impurities are most likely not the source of active carriers because the concentration of each would not be high enough in the grown matrix. For example, in one sample with an Er concentration in $In_{0.53}Ga_{0.47}As$ of $\sim 3\times 10^{19}$ cm^{-3}, the most abundant impurity in the Er source material, Pb, would exist with a maximum concentration of $\sim 10^{14}$ cm^{-3} in $In_{0.53}Ga_{0.47}As$ if all of the Pb impurity was incorporated during growth. This value is well below the concentration of active carriers for the same sample, $\sim 1\times 10^{18}$ cm^{-3}.

V. CONCLUSIONS

A systematic series of Er-doped $In_{0.53}Ga_{0.47}As$ samples was grown by MBE at 490 °C with an Er concentration of $1.5\times 10^{17}-1.4\times 10^{20}$ cm^{-3}. HAADF-STEM images and infrared absorption spectra confirmed that Er forms ErAs nanoparticles at Er concentrations $\geq 8\times 10^{19}$ cm^{-3} and is soluble in $In_{0.53}Ga_{0.47}As$ below 3.2×10^{19} cm^{-3}.

This range allows the analysis of Er as an atomic dopant and Er as an ErAs nanoparticle dopant. Temperature dependent electrical conductivity, carrier mobility, and carrier density were determined by Hall effect measurements and revealed that Er acts as a shallow donor with activation energy of ~25 meV at very dilute concentrations. This behavior is surprising given that Er is nominally isovalent with In and Ga in the host matrix. Furthermore, this work raises the possibility of using rare-earth elements for doping narrow band gap III-V semiconductors.

ACKNOWLEDGMENTS

The authors thank Oliver Bierwagen for the help with van der Pauw–Hall effect measurements, Ben Curtin for helpful discussions regarding processing of the van der Pauw samples, and John English for the help with MBE growth. This work was supported, in part, through the (U.S.) Office of Naval Research Multi-University Initiative Thermionic Energy Conversion Center, the Defense Advanced Research Projects Agency Nanostructured Materials for Power program, and the Center for Energy Efficient Materials, an Energy Frontier Research Center funded at the University of California, Santa Barbara by the Department of Energy Office of Basic Energy Sciences. A portion of this work was done in the University of California, Santa Barbara Nanofabrication Facility, part of the National Science Foundation funded by National Nanotechnology Infrastructure Network.

[1]H. Ennen and J. Schneider, in *Proceedings of the 13th International Conference on Defects in Semiconductors*, edited by L. C. Kimerling and J. M. Parsey (The Metallurgical Society of AIME, Coronado, CA, 1984), p. 115.
[2]Y. H. Xie, E. A. Fitzgerald, and Y. J. Mii, J. Appl. Phys. **70**, 3223 (1991).
[3]H. Ennen, J. Schneider, G. Pomrenke, and A. Axmann, Appl. Phys. Lett. **43**, 943 (1983).
[4]S. Coffa, F. Priolo, G. Franzo, V. Bellani, A. Carnera, and C. Spinella, Phys. Rev. B **48**, 11782 (1993).
[5]G. Zeng *et al.*, J. Electron. Mater. **37**, 1786 (2008).
[6]Robert R. Heikes and Roland W. Ure, *Thermoelectricity: Science and Engineering* (Interscience Publishers, New York, 1961), p. 576.
[7]I. Poole, K. E. Singer, and A. C. Peaker, J. Cryst. Growth **121**, 121 (1992).
[8]T. E. Buehl, J. M. LeBeau, S. Stemmer, M. A. Scarpulla, C. J. Palmstrøm, and A. C. Gossard, J. Cryst. Growth **312**, 2089 (2010).
[9]K. E. Singer, P. Rutter, A. R. Peaker, and A. C. Wright, Appl. Phys. Lett. **64**, 707 (1994).
[10]W. Kim, J. M. O. Zide, A. C. Gossard, D. O. Klenov, S. Stemmer, A. Shakouri, and A. Majumdar, Phys. Rev. Lett. **96**, 045901 (2006).
[11]W. Kim *et al.*, Appl. Phys. Lett. **88**, 242107 (2006).
[12]J. M. O. Zide, D. Vashaee, Z. Bian, G. Zeng, J. E. Bowers, A. Shakouri, and A. C. Gossard, Phys. Rev. B **74**, 205335 (2006).
[13]D. C. Driscoll, M. P. Hanson, C. Kadow, and A. C. Gossard, Appl. Phys. Lett. **78**, 1703 (2001).
[14]B. Lambert, A. L. Corre, Y. Toudic, C. Lhomer, G. Grandpierre, and M. Gauneau, J. Phys.: Condens. Matter **2**, 479 (1990).
[15]M. Hacskaylo, Phys. Status Solidi A **17**, 497 (1973).
[16]J. D. Zimmerman, E. R. Brown, and A. C. Gossard, J. Vac. Sci. Technol. B **23**, 1929 (2005).
[17]W.-K. Chu, J. W. Mayer, and M.-A. Nicolet, *Backscattering Spectrometry* (Academic, New York, NY, 1978).
[18]L. C. Feldman, *Fundamentals of Surface and Thin Film Analysis* (Elsevier Science, New York, 1986).
[19]P. M. Voyles, J. L. Grazul, and D. A. Muller, Ultramicroscopy **96**, 251 (2003).
[20]J. M. LeBeau, S. D. Findlay, L. J. Allen, and S. Stemmer, Ultramicroscopy **110**, 118 (2010).
[21]E. R. Brown, A. Bacher, D. C. Driscoll, M. P. Hanson, C. Kadow, and A. C. Gossard, Phys. Rev. Lett. **90**, 077403 (2003).
[22]A. E. Geissberger, R. A. Sadler, M. L. Balzan, and J. W. Crites, J. Vac. Sci. Technol. B **5**, 1701 (1987).
[23]S. Sethi and P. K. Bhattacharya, J. Electron. Mater. **25**, 467 (1996).
[24]M. A. Scarpulla, J. M. O. Zide, J. M. LeBeau, C. G. Van De Walle, A. C. Gossard, and K. T. Delaney, Appl. Phys. Lett. **92**, 173116 (2008).
[25]J. M. O. Zide, D. O. Klenov, S. Stemmer, A. C. Gossard, G. Zeng, J. E. Bowers, D. Vashaee, and A. Shakouri, Appl. Phys. Lett. **87**, 112102 (2005).
[26]D. O. Klenov, J. M. O. Zide, J. M. LeBeau, A. C. Gossard, and S. Stemmer, Appl. Phys. Lett. **90**, 121917 (2007).
[27]D. D. Nolte, J. Appl. Phys. **76**, 3740 (1994).
[28]M. P. Hanson, A. C. Gossard, and E. R. Brown, J. Appl. Phys. **102**, 043112 (2007).
[29]O. Stenzel, J. Cluster Sci. **10**, 169 (1999).
[30]J. R. Heath, Phys. Rev. B **40**, 9982 (1989).
[31]Z. L. Wang and J. M. Cowley, Ultramicroscopy **23**, 97 (1987).
[32]M. Blaber, M. Arnold, N. Harris, M. Ford, and M. Cortie, Physica B **394**, 184 (2007).
[33]J. J. Mock, D. R. Smith, and S. Schultz, Nano Lett. **3**, 485 (2003).
[34]J. Serre and A. Ghazali, Phys. Rev. B **28**, 4704 (1983).
[35]H. C. Casey, D. D. Sell, and K. W. Wecht, J. Appl. Phys. **46**, 250 (1975).
[36]P.-O. Holtz and Q. X. Zhao, *Impurities Confined in Quantum Structures* (Springer, New York, 2004), pp. 8–10.
[37]SHIVA Technologies, GDMS Analytical Report for Er Source Material from AMES Laboratory (Syracuse, NY, 2008), p. 1.